Nonlinear Dyn (2016) 86:501–512
DOI 10.1007/s11071-016-2903-1

ORIGINAL PAPER

Nonlinear dynamic analysis of wire-rope isolator and Stockbridge damper

Nilson Barbieri · Renato Barbieri · Rodrigo Aparecido da Silva · Marcos José Mannala · Lucas de Sant'Anna Vitor Barbieri

Received: 30 November 2015 / Accepted: 15 June 2016 / Published online: 30 June 2016

Abstract The Bouc–Wen model was used to investigate nonlinear dynamical behavior of a wire-rope isolator and an asymmetric Stockbridge damper. The experimental vibration signals were acquired through accelerometers placed along the sample. The wire-rope isolator system was excited using and electromechanical shaker with constant values of acceleration, and the Stockbridge damper was excited using a cam machine with different profiles. The numeric and experimental data were approximated using particle swarm optimization method. The agreement between numerical and experimental data show that the model of Bouc–Wen is well suited for dynamic analysis of such systems.

Keywords Wire-rope isolator · Stockbridge damper · Vibration · Bouc–Wen model

N. Barbieri (✉) · R. A. da Silva · M. J. Mannala · L. de S. V. Barbieri
Pontifícia Universidade Católica do Paraná– PUCPR, Rua Imaculada Conceição, 1155, Curitiba, Paraná CEP 80215-901, Brazil
e-mail: nilson.barbieri@pucpr.br

N. Barbieri
Universidade Tecnológica Federal do Paraná -UTFPR, Curitiba, Brazil

R. Barbieri
Faculdade de Engenharia de Joinville -FEJ, Joinville, Brazil

1 Introduction

A recent survey of the hysteresis Bouc–Wen Model [5,31] can be found in [16]. The nonlinear behavior of the systems with hysteresis are encountered in a wide variety of processes in which the input–output dynamic relations between variables involve memory effects. Examples are found in biology, optics, electronics, ferroelectricity, magnetism, mechanics, structures, among other areas. In mechanical and structural systems, hysteresis appears as a natural mechanism of materials to supply restoring forces against movements and dissipate energy. In these systems, hysteresis refers to the memory nature of inelastic behavior where the restoring force depends not only on the instantaneous deformation, but also on the history of the deformation. The detailed modeling of these systems using the laws of Physics is an arduous task, and the obtained models are often too complex to be used in practical applications involving characterization of systems, identification or control [16].

The Bouc–Wen model for smooth hysteresis has received an increasing interest in the last few years due to the ease of its numerical implementation and its ability to represent a wide range of hysteresis loop shapes. This model consists of a first-order nonlinear differential equation that contains some parameters that can be chosen, using identification procedures, to approximate the behavior of given physical hysteretic system [13–16].

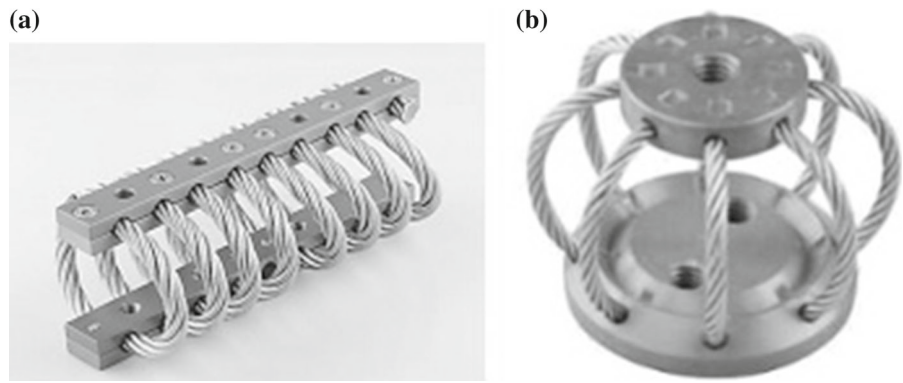

Fig. 1 Wire ropes: **a** Helical isolator [2]. **b** Polycal isolator [2]

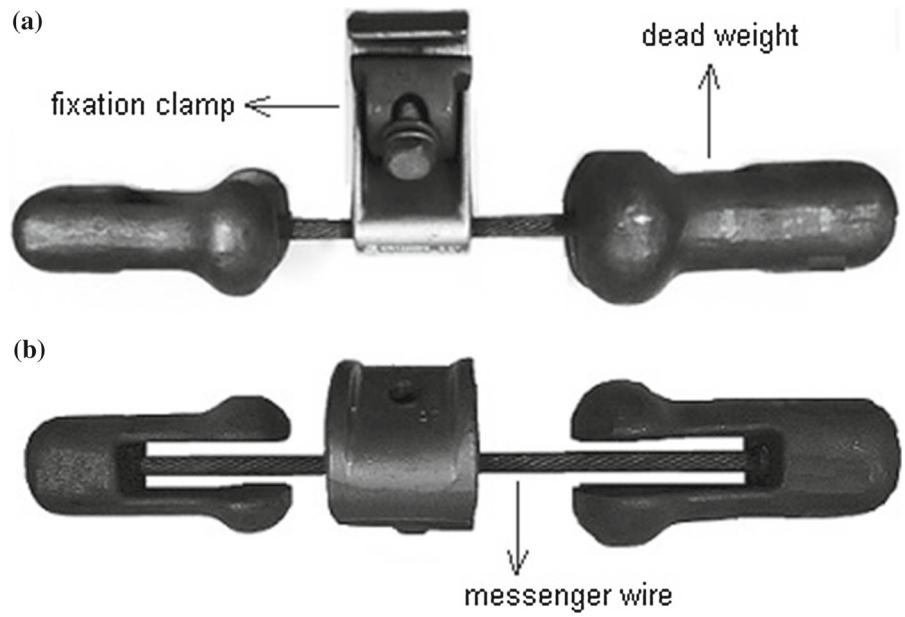

Fig. 2 Stockbridge damper. **a** Front view and **b** top view

Efficient formulations for the response and dissipated energy of Bouc–Wen hysteretic model are shown in [6–11,13–16,18–20,22,24,26,27,32].

Wire cable vibration isolators (Fig. 1) are typical nonlinear hysteretic damping devices, which have the advantages of large resonant damping, good capabilities in resisting heat and corrosion, etc.

Under large structural deformation, they exhibit softening or soft-hardening stiffness property. Therefore, wire cable vibration isolators are able to absorb efficiently impact energy and provide broadband vibration isolation. In the past decade, they have been applied widely in the engineering fields such as aerospace, ship, civil engineering and automobile. As the damping is exerted by sliding, rubbing and extruding among wire strands, the hysteretic properties of restoring force-deformation for wire cable isolators are similar with that of stress–strain for elastoplastic material. It is important for response prediction and design improvement of isolation systems to identify accurately the hysteretic restoring forces of wire cable vibration isolators [12]. Several applications of this vibration isolation mechanism can be found at [1,2,6–8,12,25,29,30].

The Stockbridge damper [28] (Fig. 2) is presently the most common type of transmission line damper. In general, the absorber consists of two weights attached to the end of stranded cables, which are known as *messenger wires*.

In Stockbridge dampers of transmission line, mechanical energy is dissipated in wire cables (damper or messenger cables). The damping mechanism is due to statical hysteresis resulting from Coulomb (dry) fric-

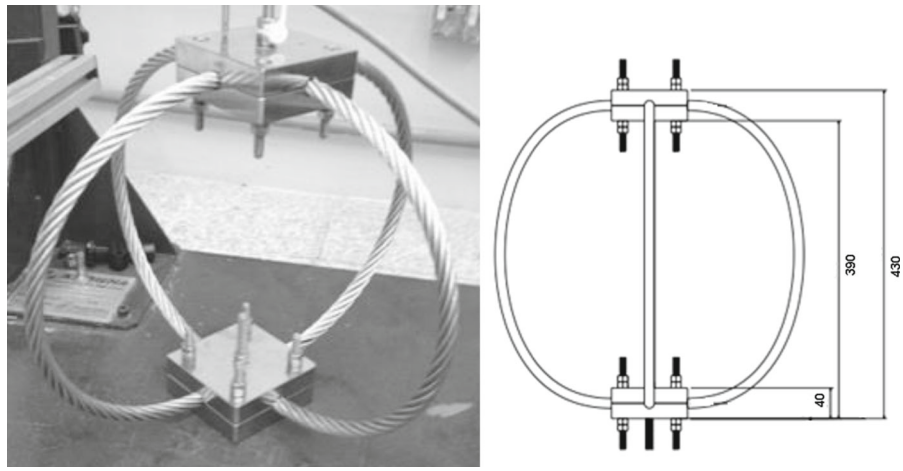

Fig. 3 Prototype wire-rope isolator system and geometric data

tion between the individual wires of the cable undergoing bending deformation. In order to test this dynamical model of Stockbridge damper, the typical experimental impedance curves are compared with numeric results. This procedure is vastly used considering the Masing model for modeling the nonlinear damping behavior of the damper cable of the Stockbridge damper [3]. Nonlinear mathematical models for simulating the dynamic behavior of Stockbridge damper can be found in [3,4,23].

PSO is a population-based stochastic optimization technique developed by Eberhart and Kennedy in [17], inspired by social behavior of bird flocking or fish schooling. Sometimes it is related to the Evolutionary Computation (EC) techniques, basically with Genetic Algorithms (GA) and Evolutionary Strategies (ES), but there are significant differences with those techniques. The PSO algorithm is population-based: a set of potential solutions evolves to approach a convenient solution (or set of solutions) for a problem. Being an optimization method, the aim is finding the global optimum of a real-valued function (fitness function) defined in a given space (search space).

In this work, the physical parameters used in a Bouc–Wen model are adjusted using PSO method through the comparison between numerical and experimental results for two different systems: wire-rope isolator and Stockbridge damper. The numerical model of a Stockbridge damper is obtained using the Finite Element Method. The experimental results are obtained using an electromechanical shaker (with constant acceleration) or a cam machine with five different eccentricities (constant displacement). The experimental results are compared with nonlinear numerical results. The nonlinear system contains nonlinear stiffness and damping elements.

2 Mathematical models

2.1 Wire-rope isolator

The Bouc–Wen model has been widely used to describe nonlinear hysteretic systems. The differential equation model is phenomenological and reflects local memory-dependent hysteresis. For a given time history of the displacement, the hysteretic restoring force can be completely specified by this analytical model. The left side of Fig. 3 shows the built prototype and in the right side the geometric dimensions (in mm) .The wire-rope prototype consists of four identical steel bases with masses of 1.3 kg, four steel cables of 0.5 in. diameter and four stainless steel screws. The prototype was built without taking into account specific technical considerations. They were simply used components available on the market (cable) and screws.

Figure 4 shows the equivalent sdof (single degree-of-freedom) system used by [21]. The system consists of a wire-rope isolator with restoring force $F(t)$ and a mass M on top of the isolator. The excitation $u(t)$ is applied to the base of the isolator through an electromechanical shaker. Hence, the wire-rope deflection $d(t)$ is determined by the difference between position of the mass $x(t)$ and base displacement $u(t)$, that is $d(t) = x(t) - u(t)$. The equation of motion is:

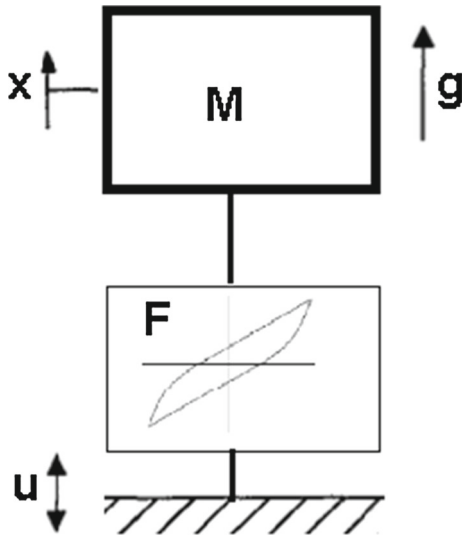

Fig. 4 Single degree-of-freedom model

$$M\ddot{x}(t) = -F(d, \dot{d}, z, t) + Mg \tag{1}$$

The differential motion equation with three state variables: $x_1 = x$;$x_2 = \dot{x}$ and $x_3 = z$, is:

$$\begin{pmatrix} \dot{x} \\ \ddot{x} \\ \dot{z} \end{pmatrix} = \begin{pmatrix} x_2 \\ \frac{1}{M}\left[-b^{cd}\left[x_3 + k_1 d + k_2 d^2 \text{sign}(d) + k_3 d^3\right]\right] \\ \dot{d}\left[\alpha - \left[\gamma + \beta \text{sign}(\dot{d})\text{sign}(x_3)\right]|x_3|^n\right] \end{pmatrix} \tag{2}$$

The term b^{cd} is used as a sort of shaping function, which also assures the hardening overlapping loading envelope, in this case, b and c are parameter to be adjusted and d is the relative displacement between $x(t)$ and $u(t)$.

In this case was used the Bouc–Wen model expressed by

$$\dot{z} = \alpha\dot{x}(t) - \beta\,|\dot{x}(t)|\,z(t)\,|z(t)|^{n-1} - \gamma\dot{x}(t)\,|z(t)|^n \tag{3}$$

where $x(t)$ is the displacement and $z(t)$ is the hysteretic force; $b, c, \alpha, \beta, \gamma, k_1, k_2, k_3$ and n are model parameters. The slope of the hysteresis loops governed by the Bouc–Wen model can be derived as

$$\frac{\mathrm{d}z}{\mathrm{d}x} = \alpha - \left[\gamma + \beta\,\text{sign}(\dot{x})\text{sign}(z)\right]|z(t)|^n \tag{4}$$

2.2 Stockbridge damper

To obtain the mathematical model of the Stockbridge damper system [3] is necessary to analyze separately the components showed in Fig. 5.

The messenger wire is modeled by the Euler–Bernoulli beam finite element. In this element, the transversal displacement is interpolated using the well-known *Hermitian interpolation polynomials* with C^1 continuity, and the degrees of freedom (df) in each node are the transversal displacement and the rotation, $\{v,\theta\}$. The dynamic equation for this element can be written as:

$$\begin{aligned} &\frac{\rho AL}{420}\begin{bmatrix} 156 & 22L & 54 & -13L \\ & 4L^2 & 13L & -3L^2 \\ & & 156 & -22L \\ \text{sym.} & & & 4L^2 \end{bmatrix}\begin{Bmatrix} \ddot{v}_1 \\ \ddot{\theta}_1 \\ \ddot{v}_2 \\ \ddot{\theta}_2 \end{Bmatrix} \\ &+\frac{EI}{L^3}\begin{bmatrix} 12 & 6L & -12 & 6L \\ & 4L^2 & -6L & 2L^2 \\ & & 12 & -6L \\ \text{sym.} & & & 4L^2 \end{bmatrix}\begin{Bmatrix} v_1 \\ \theta_1 \\ v_2 \\ \theta_2 \end{Bmatrix} \\ &= -\frac{\rho AL}{12}\begin{Bmatrix} 6 \\ L \\ 6 \\ -L \end{Bmatrix}\ddot{y}_0 \end{aligned} \tag{5}$$

where ρA is the linear density of the cable, L is the finite element length, EI is the cable flexural (bending) stiffness, and $\ddot{y}_0$ is the base acceleration (the acceleration imposed by the cam machine).

The suspended masses of the Stockbridge damper are modeled with a rigid body plane motion hypothesis, and the admissible displacements are shown in Fig. 5.

After assembling all the elements of the messenger wire, each weight of the Stockbridge damper contributes to two terms of the dynamical equilibrium. The first contribution is in the mass matrix (inertia force)

$$[M_S]\{\ddot{q}_n\} = \begin{bmatrix} m & m\bar{x} \\ m\bar{x} & I_n \end{bmatrix}\begin{Bmatrix} \ddot{v}_n \\ \ddot{\theta}_n \end{Bmatrix} \tag{6}$$

and another parcel is in the vector force due to base acceleration

$$\{f_s\} = -\begin{Bmatrix} m \\ m\bar{x} \end{Bmatrix}\ddot{y}_0 \tag{7}$$

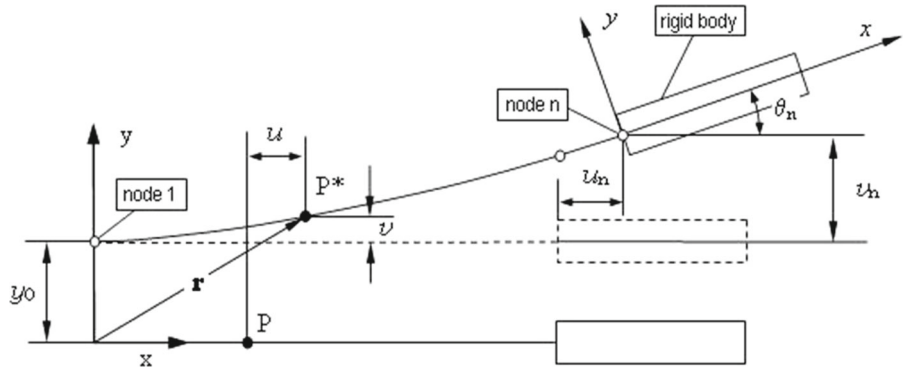

Fig. 5 References and admissible displacements

where m is the mass of the Stockbridge damper weight, $\bar{x}$ is the center of mass coordinate and I_n is the inertia moment with the reference fixed in node n.

The Stockbridge damper dynamical equilibrium equation is obtained after assembling all finite elements, and it can be conventionally written as

$$[M]\{\ddot{q}\} + [K]\{q\} = \{f_0\}\,\ddot{y}_0(t) \tag{8}$$

where $[M]$ and $[K]$ are the mass and stiffness matrices, respectively, and $\{f_0\}$ is the force vector. The vector components $\{q\}$ are the finite element node displacements and rotations, v and θ, and $\ddot{y}_0$ is the acceleration in node 1 (base shaker acceleration).

In order to take into consideration the cable *hysteretic damping* in Eq. (8), it is enough to consider the flexural stiffness as:

$$EI = EI_0(1 + \eta i) \tag{9}$$

where η is the *hysteretic damping constant* and $i = \sqrt{-1}$.

The nonlinear system model can be obtained including the cubic stiffness matrix in (8):

$$[M]\{\ddot{q}\} + [K_1]\{q\} + [K_3]\{q^3\} = \{f_0\}\,\ddot{y}_0(t) \tag{10}$$

To simplify the mathematical model and the computational simulations, it was considered only the main diagonal of the nonlinear stiffness matrix $[K_3]$.

3 Results

3.1 Wire-rope isolator

The experimental vibration data of wire-rope isolator were obtained taking account different base excitation levels of constant acceleration varying from 0.1 to 1 m/s^2 with increment of 0.1 m/s^2(step sine). The electromechanical shaker was used in the step sine test with the frequency range varied from 8 to 25 Hz with an increment of 0.12 Hz. Two accelerometers were used to collect the vibration data. One accelerometer was placed at the base excitation point (input signal) and the second accelerometer at the other base. Computational routines were developed in MATLAB for simulation of differential equations. The numeric signals were obtained in the time domain and were considered only the stationary signals to obtain the difference $d_{\max} - d_{\min}$ (without initial transitory part). Figure 6 shows the experimental curves of acceleration for ten steps with constant values of the base acceleration.

The frequency–response curves show clearly the nonlinear behavior of the wire-rope isolator. The harmonic resonance frequency shifts to the left for increasing amplitude of excitation, indicating softening stiffness. The isolator was tested up to very large deformations. It was observed that the isolator exhibited asymmetric hysteresis loops, and the asymmetry was enhanced with an increase in displacement amplitude. Both the effective stiffness and the energy dissipation of the wire-rope isolator decrease when the amplitude of excitation increases [21]. It is possible to notice that the peak value varies according the amplitude of the base

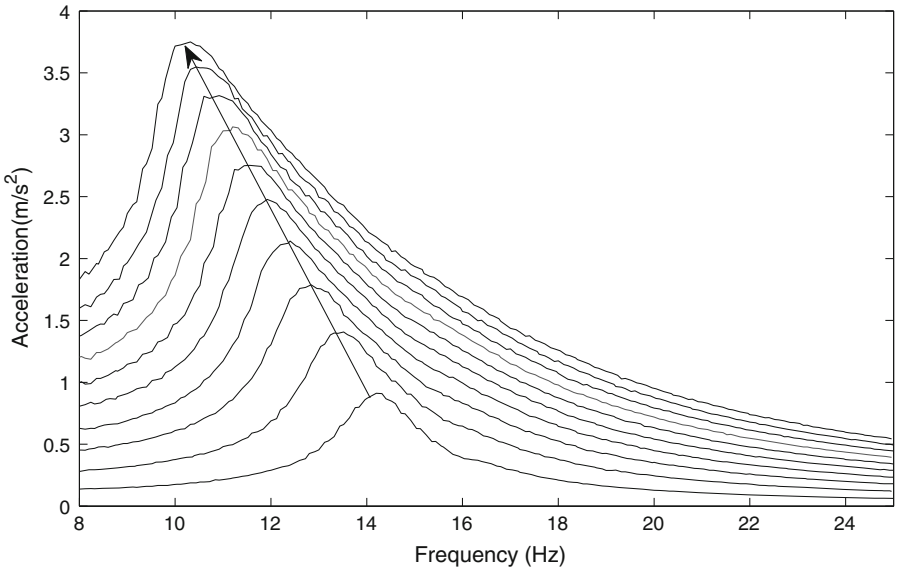

Fig. 6 Acceleration amplitude (experimental data). Each curve represents one level of base acceleration varying from 0.1 to 1 m/s^2 with increment of 0.1 m/s^2. The amplitude peaks increase with increasing acceleration level

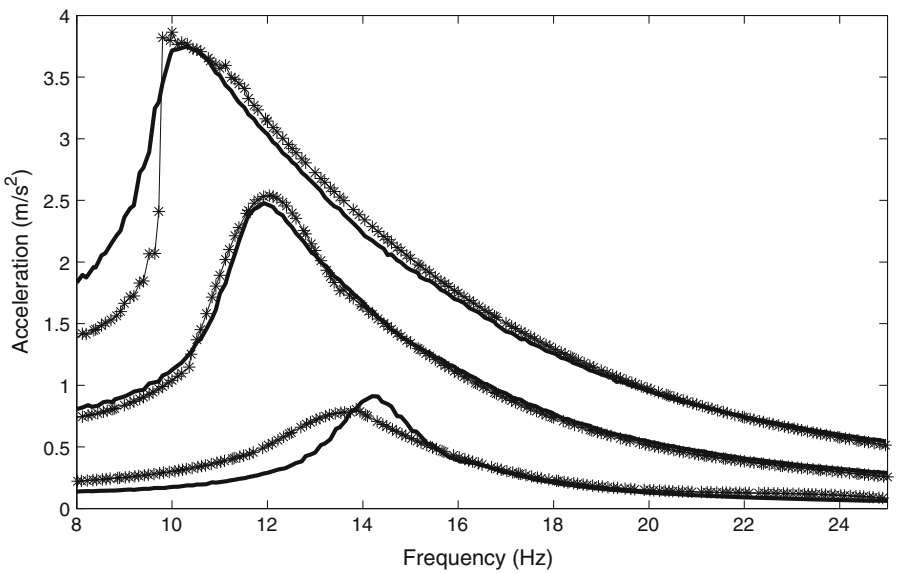

Fig. 7 Acceleration amplitude (experimental data—*solid line*; adjusted data—*solid line with symbol asterisk*)

acceleration. For base acceleration of 0.1 m/s^2, the peak value is obtained in 14.2 Hz and for base acceleration of 1.0 m/s^2 the peak value is obtained in 10.32 Hz.

Satisfactory results were obtained using the PSO method to make the approximation of the numeric and experimental values. The PSO parameters used in this application are: particles number = 20; iterations = 150; acceleration constants = [2.1; 2.1]; inertia weights = [0.9;0.6];. The global objective function is defined by:

$$f = \sum_{j=1}^{\mathrm{nc}} \left(\sum_{i=1}^{\mathrm{np}} \left| A_{\mathrm{exp.}} - A_{\mathrm{FEM}} \right| \right) \tag{11}$$

where A_{exp} is the experimental acceleration amplitude; A_{FEM} is the same numeric acceleration amplitude estimated using PSO; and np is the number of points (normally np varies from 50 to 100 points around the peak values of the curves); nc is the number of experimental curves (in this case nc = 10).

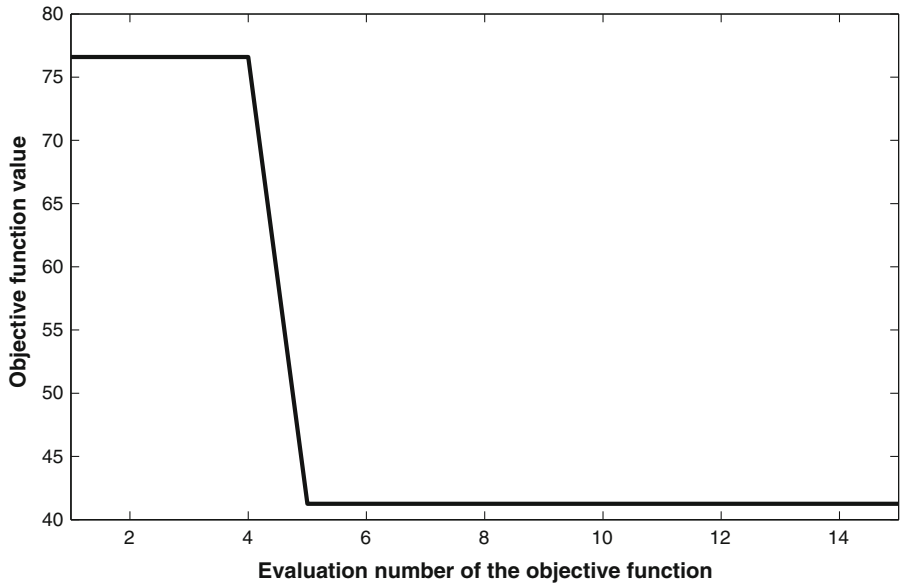

Fig. 8 Objective function value

Table 1 Optimized parameters of the Bouc–Wen model

k1 (N/m)	b (–)	c (m^{-1})	α (N/m)	β (N^{1-n}/m)	γ (N^{1-n}/m)	n (–)	k_3 (N/m^3)
6781.8	2.523	1863.45	546.52	1083.25	−27,311.31	0.0062	2.152×10^{10}

Figure 7 shows the adjusted numeric curves for three values of base acceleration of 0.1, 0.5 and 1 m/s^2 and the corresponding experimental curves. Figure 8 shows the variation of the objective function. It can be noted that the values of experimental and numeric curves have good agreement. The great differences occur for low and high values of base acceleration. The objective function rapidly converges to the final value. This fact is due to previously adjustment of the initial values of the optimized parameters showed in Table 1.

Figure 9 shows the adjusted numeric curves of acceleration for ten steps with constant values of the base acceleration. In Table 1 are shown the optimized parameters using the Bouc–Wen model. The k_2 parameter was neglected in all analysis. It is clear in Fig. 7 and comparing the curves of Figs. 6 and 9 that the curves obtained for the larger excitation levels exhibit jump that is probably due to an unstable behavior. The experimental curves do not show jumps. The experimental response is more damped with respect to numerical identification. This fact may be related with the signal acquisition system that failed to capture these variations (jumps).

Figure 10 shows the restoring force $F(d, \dot{d}, z, t)$ presents in the right side of Eq. (1) for three values of base acceleration of 0.1, 0.5 and 1 m/s^2 with identified parameters of Table 1 at the displacement amplitudes corresponding to maximum resonance response of Fig. 7. The frequencies used are 10.0, 12.04 and 13.86 Hz.

3.2 Stockbridge damper

Figure 11 [3] shows the schematic representation of the machine cam used in the experimental testing of the Stockbridge damper with controlled oscillation (displacement). The experimental data are obtained through three accelerometers placed in the half sample. One accelerometer was placed in the center (A2) and another at the end of the messenger wire (A3). A third accelerometer (reference) was placed on the connecting rod (A1).

Figure 12 shows the cam machine with Stockbridge damper coupled and two accelerometers positioned on the weight. The data acquisition system is composed

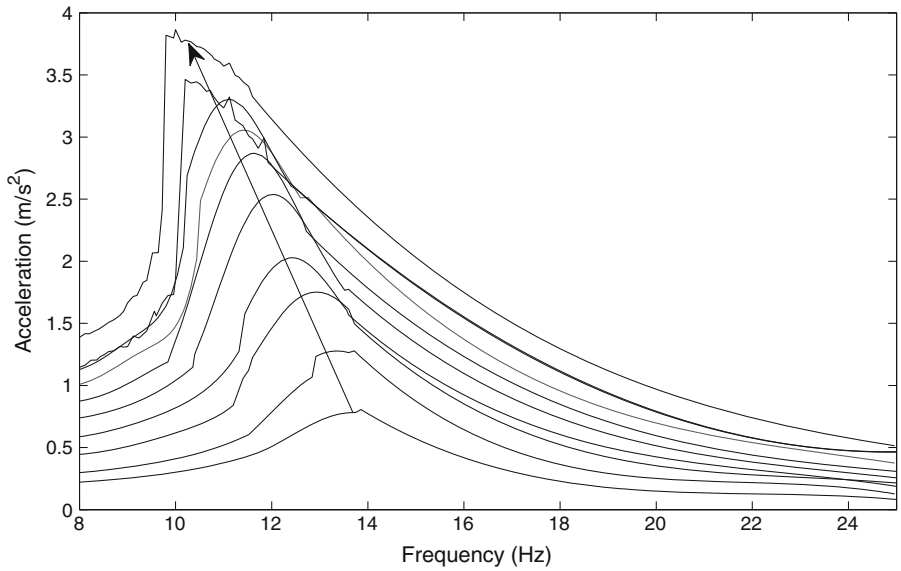

Fig. 9 Acceleration amplitude (numeric data). *Each curve* represents one level of base acceleration varying from 0.1 to 1 m/s^2 with increment of 0.1 m/s^2. The amplitude peaks increase with increasing acceleration level

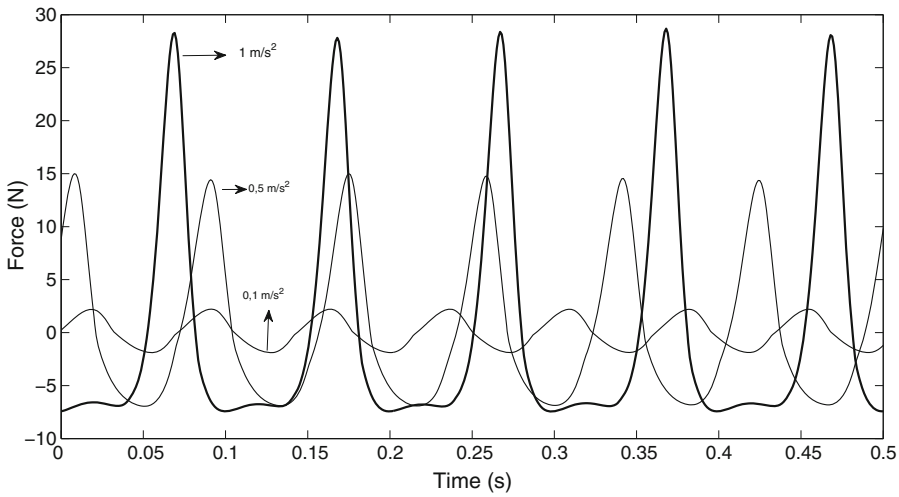

Fig. 10 Restoring force with three levels of base acceleration (0.1, 0.5 and 1 m/s^2)

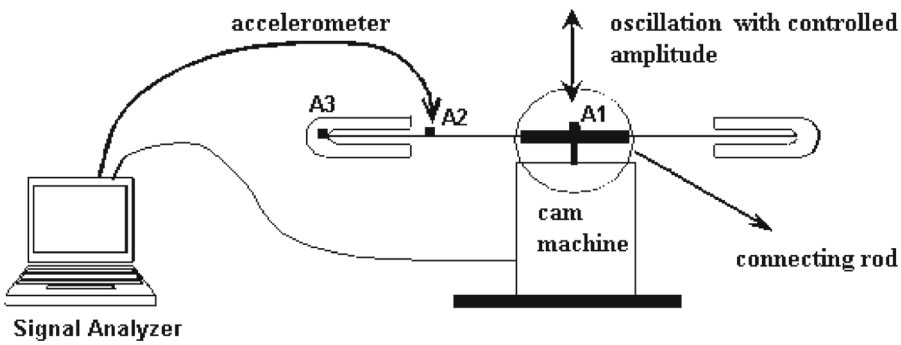

Fig. 11 Schematic cam machine

of a signal analyzer (HP 3567) and modal accelerometers (PCB 333AX, sensitivity ≈100 mv/g). The cam machine with radial flat-faced follower is manually operated.

Five different disk cams with eccentricities of 0.25, 0.5, 0.75, 1.25, 1.5 mm were used. The tests were carried out varying the excitation frequency between 5 and 17 Hz with increments of 0.25 Hz. This lower fre-

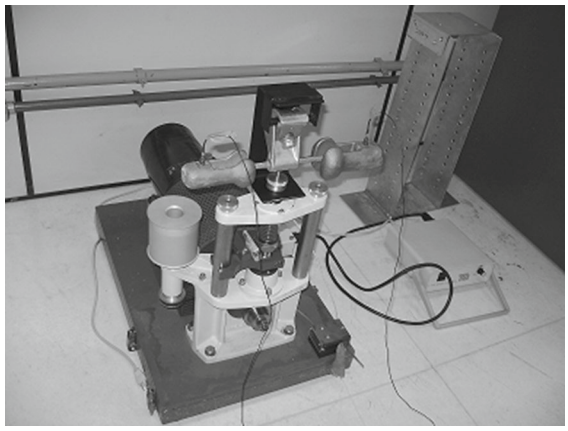

Fig. 12 Cam machine with Stockbridge coupled

quency range was used due to the mechanical limitation of the excitation system. Figure 13 shows the experimental curves of the acceleration ratio obtained for the accelerometer at the end (accelerometer 2) of the messenger wire. The natural frequency changes with the variation of the amplitude of the input signal (base excitation).

Excellent results were obtained using the PSO to make the approximation of the numeric and experimental values. The PSO parameters used in this application are: particles number = 20; iterations = 150; acceleration constants = [2.1; 2.1]; inertia weights = [0.9;0.6];. The objective function is defined by:

$$f = \sum_{i=1}^{\mathrm{np}} \left| Paa_{\mathrm{exp.}} - Paa_{\mathrm{FEM}} \right| \tag{12}$$

where Paa_{exp} is the acceleration ratio (acceleration of the reference sensor/acceleration of the accelerometer on the cable); Paa_{FEM} is the same acceleration ratio estimated using PSO; and np is the number of points (normally np = 47);

Figure 14 shows the numeric adjusted curves of the acceleration ratio obtained for the position of the accelerometer at the end (accelerometer 2) of the messenger wire.

In Table 2 are shown the optimized parameters using the Bouc–Wen model. The parameters were adjusted separately for each eccentricity of the cam. The variation of the parameter EI (flexural stiffness) and the loss factor η with the variation of the base displacement can be noted.

Figure 15 shows the adjusted numeric curves for three values of base displacement of 0.25, 0.75 and 1.5 mm and the corresponding experimental curves. Figure 16 shows the variation of the objective function for the case in which the base excitation is 0.25 mm. It can be noted that the values of experimental and numeric curves have good agreement. The objective function rapidly converges to the final value. Similar curves are obtained for the other cases of base excitation

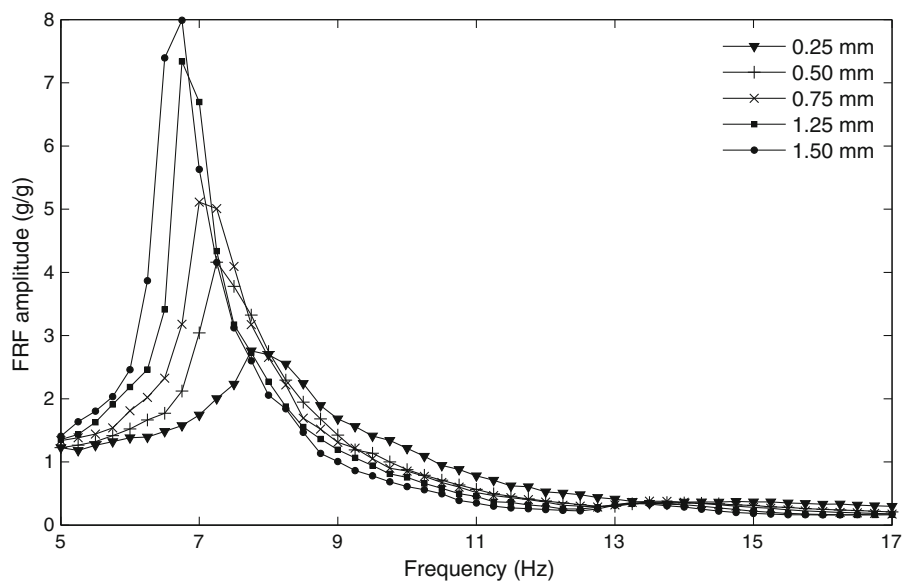

Fig. 13 Acceleration ratio curves of accelerometer 2 (experimental data)

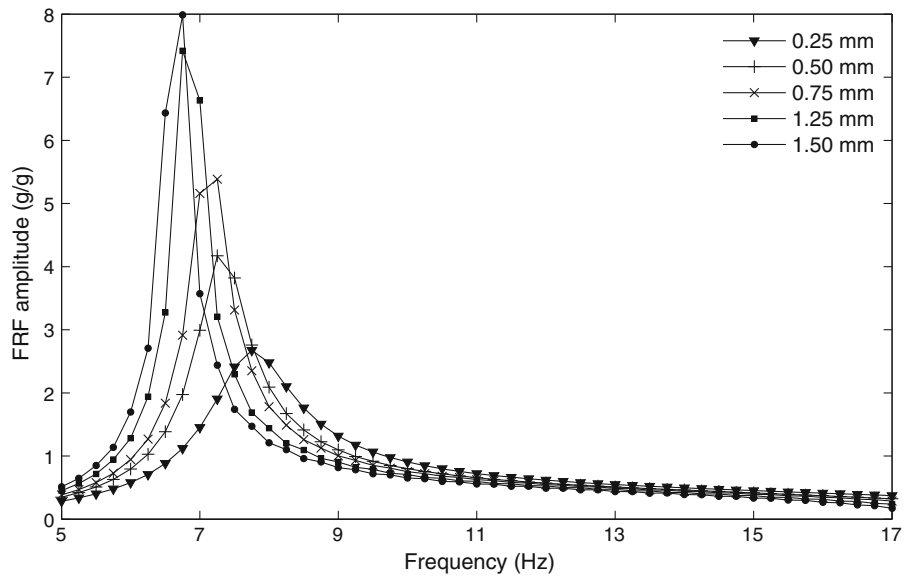

Fig. 14 Acceleration ratio curves of accelerometer 2 (numeric data)

Table 2 Optimized parameters of the Bouc–Wen model

Ecc. (mm)	EI (Nm^2)	η	b (–)	c m^{-1}	α (N/m)	β (N^{1-n}/m)	γ (N^{1-n}/m)	n (–)	k_3 (N/m^3)
0.25	1.9393	0.1472	0.5643	0.1100	1.6433	0.8151	−0.6382	10.8945	2.1655×10^3
0.50	1.7484	0.0912	0.6012	0.1118	1.3996	0.9595	−0.5826	10.5954	2.2084×10^3
0.75	1.6654	0.0656	0.6640	0.1279	1.2226	0.9295	−0.7439	12.1188	1.3816×10^3
1.25	1.5454	0.0472	0.6668	0.1312	1.6941	0.8930	−0.6186	8.2112	2.2566×10^3
1.50	1.4546	0.0413	0.6591	0.1241	1.0918	0.7676	−0.6113	11.3392	1.3150×10^3

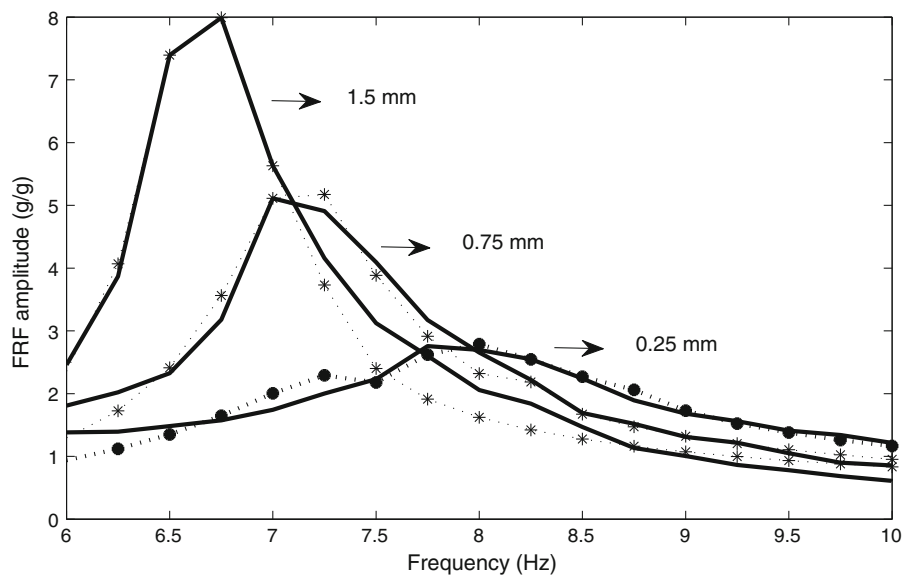

Fig. 15 FRF amplitude (experimental data—*solid line*; adjusted data—*dotted line with symbol asterisk*)

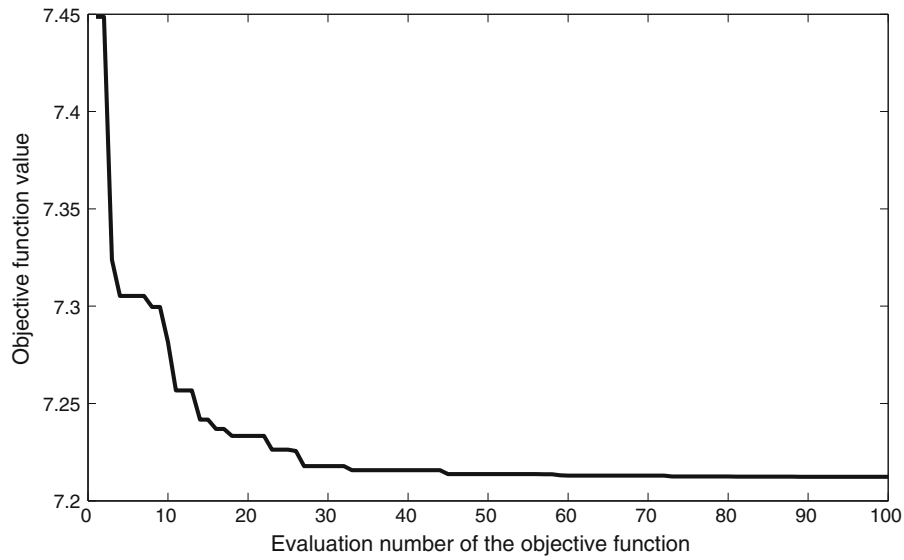

Fig. 16 Objective function value

4 Conclusion

In this work, the physical parameters used in a Bouc–Wen model were adjusted using PSO method through the comparison between numerical and experimental results for two different systems: wire-rope isolator and Stockbridge damper

For both systems was possible to adjust the parameters used in the mathematical model of Bouc–Wen. The results show that fine adjustments were efficient, i.e., the numerical and experimental results are close.

A global objective function was set to wire-rope model taking into account the experimental data obtained for ten different constant acceleration values from the base excitation. The great differences occurs for low and high values of base acceleration. The objective function rapidly converges to the final value. The frequency–response curves show clearly the nonlinear behavior of the wire-rope isolator. The harmonic resonance frequency shifts to the left for increasing amplitude of excitation, indicating softening stiffness.

The objective function to adjust the Bouc–Wen model parameters and the linear flexural stiffness was applied separately for five different vibration data obtained to five displacements of the base excitation of a Stockbridge model. The frequency–response curves show clearly the nonlinear behavior of the Stockbridge damper. The harmonic resonance frequency shifts to the left for increasing amplitude of excitation, indicating softening stiffness. The results showed that the flexural stiffness and the loss factor varies with the base displacement.

References

1. Balaji, P.S., Moussa, L., Rahman, M.E., Vuia, L.T.: Experimental investigation on the hysteresis behavior of the wire rope isolators. J. Mech. Sci. Technol. **29**(4), 1527–1536 (2015)
2. Balaji, P.S., Rahman, M.E., Moussa, L., Lau, H.H.: Wire rope isolators for vibration isolation of equipment and structures—a review. IOP conference series. Materials Science and Engineering **78**, 1–10 (2015)
3. Barbieri, N., Barbieri, R.: Dynamic analysis of Stockbridge damper. Adv. Acoust. Vib. **2012**, 1–8 (2012)
4. Barry, O., Zu, J.W., Oguamanam, D.C.D.: Nonlinear dynamics of Stockbridge dampers. J. Dyn. Syst. Meas. Control **137**(6), 1–7 (2015)
5. Bouc, R.: Forced vibration of mechanical systems with hysteresis. In: Proceedings of the Fourth Conference on Nonlinear Oscillation, Prague, Czechoslovakia (1967)
6. Carboni, B., Lacarbonara, W., Aurichio, F.: Hysteresis of multiconfiguration assemblies of nitinol and steel strands: experiments and phenomenological identification. J. Eng. Mech. **141**(3), 1–16 (2015)
7. Carboni, B., Lacarbonara, W.: Nonlinear dynamic characterization of a new hysteretic device: experiments and computations. Nonlinear Dyn. **83**(1), 23–29 (2016)
8. Carboni, B., Mancini, C., Lacarbonara, W.: Hysteretic Beam Model for Steel Wire Ropes Hysteresis Identification. Structural Nonlinear Dynamics and Diagonosis. Springer, Berlin (2015)
9. Charalampakis, A.E., Koumousis, V.K.: Identification of Bouc–Wen hysteretic systems by a hybrid evolutionary algorithm. J. Sound Vib. **314**, 571–585 (2008)

10. Charalampakis, A.E., Dimou, C.K.: Identification of Bouc–Wen hysteretic systems using particle swarm optimization. Comput. Struct. **88**, 1197–1205 (2010)
11. Charalampakis, A.E., Koumousis, V.K.: On the response and dissipated energy of Bouc–Wen hysteretic model. J. Sound Vib. **309**, 887–895 (2008)
12. Chungui, Z., Xinong, Z., Shilin, X., Tong, Z., Changchun, Z.: Hybrid modeling of wire cable vibration isolation system through neural network. Math. Comput. Simul. **79**, 3160–3173 (2009)
13. Ikhouane, F., Hurtado, J.E., Rodellar, J.: Variation of the hysteresis loop with the Bouc–Wen model parameters. Nonlinear Dyn. **48**, 361–380 (2007)
14. Ikhouane, F., Rodellar, J.: On the hysteretic Bouc–Wen model. Part I: forced limit cycle characterization. Nonlinear Dyn. **42**, 63–78 (2005)
15. Ikhouane, F., Rodellar, J.: On the hysteretic Bouc–Wen model. Part II: robust parametric identification. Nonlinear Dyn. **42**, 79–95 (2005)
16. Ismail, M., Ikhouane, F., Rodellar, J.: The hysteresis Bouc–Wen model—a survey. Arch. Comput. Methods Eng. **16**, 161–188 (2009)
17. Kennedy, J., Eberhart, RC.: Particle swarm optimization. IEEE International Conference on Neural Networks, Perth, Australia (1995)
18. Kyprianou, A., Worden, K.: Identification of hysteretic systems using the differential evolution algorithm. J. Sound Vib. **248**(2), 289–314 (2001)
19. Lacarbonara, W., Vestroni, F.: Nonlinear phenomena in hysteretic systems. Proc. IUTAM **5**, 69–77 (2012)
20. Lacarbonara, W., Vestroni, F.: Nonclassical responses of oscillators with hysteresis. Nonlinear Dyn. **32**, 235–258 (2003)
21. Leenen, R.: The Modelling and Identification of an Hysteretic System—The Wire-Rope as a Nonlinear Shock Vibration Isolator. Technical report. DCT 2002.72, Eindhoven University of Technology, 44 p (2002)
22. Li, H.G., Meng, G.: Nonlinear dynamics of a SDOF oscillator with Bouc–Wen hysteresis. Chaos Solitons Fractals **34**, 337–343 (2007)
23. Luo, X., Wang, L., Zhang, Y.: Nonlinear numerical model with contact for Stockbridge vibration damper and experimental validation. J. Vib. Control **22**(5), 1217–1227 (2016)
24. Ni, Y.Q., Ko, J.M., Wong, C.W.: Identification of non-linear hysteretic isolators from periodic vibration tests. J. Sound Vib. **217**, 737–756 (1998)
25. Pagano, S., Strano, S.: Wire rope springs for passive vibration control of a light steel structure. WSEAS Trans. Appl. Theor. Mech. **3**, 212–221 (2013)
26. Pozo, F., Acho, L., Rodríguez, A., Pujol, G.: Nonlinear modeling of hysteretic systems with double hysteretic loops using position and acceleration information. Nonlinear Dyn. **57**, 1–12 (2009)
27. Rochdi, Y., Giri, F., Ikhouane, F., Chaoui, F.Z., Rodellar, J.: Parametric identification of nonlinear hysteretic systems. Nonlinear Dyn. **58**, 393–404 (2009)
28. Stockbridge, GH.: "Vibration damper," U.S. Patent No. 1,675,391 (1928)
29. Tinker, M.L., Cutchins, M.A.: Damping phenomena in a wire rope vibration isolation system. J. Sound Vib. **157**(1), 7–18 (1992)
30. Wang, H.X., Gong, X.S., Pan, F., Dang, X.J.: Experimental investigations on the dynamic behaviour of o-type wire-cable vibration isolators. Shock Vib. **2015**, 1–12 (2015)
31. Wen, Y.: Method for random vibration of hysteretic systems. J. Eng. Mech. Div. **102**(2), 249–263 (1976)
32. Ye, M., Wang, X.: Parameter estimation of the Bouc–Wen hysteresis model using particle swarm optimization. Smart Mater. Struct. **16**, 2341–2349 (2007)